

Article

T-FSW of Dissimilar Aerospace Grade Aluminium Alloys: Influence of Second Pass on Weld Defects

Mustufa Haider Abidi ^{1,*}, Nabeel Ali ², Hashmatullah Ibrahimi ², Saquib Anjum ², Dhruv Bajaj ², Arshad Noor Siddiquee ², Mohammed Alkahtani ^{1,3} and Ateekh Ur Rehman ³

¹ Advanced Manufacturing Institute, King Saud University, Riyadh 11421, Saudi Arabia; moalkahtani@ksu.edu.sa

² Department of Mechanical Engineering, Jamia Millia Islamia, New Delhi 110025, India; nabeelali22@gmail.com (N.A.); hashmatullahibrahimi.hi@gmail.com (H.I.); saquibanjum98@gmail.com (S.A.); maildhruv08@gmail.com (D.B.); ansiddiqui@jmi.ac.in (A.N.S.)

³ Industrial Engineering Department, College of Engineering, King Saud University, Riyadh 11421, Saudi Arabia; arehman@ksu.edu.sa

* Correspondence: mabidi@ksu.edu.sa; Tel.: +966-545269756

Received: 28 March 2020; Accepted: 17 April 2020; Published: 18 April 2020



Abstract: The restoration of numerous aircraft structures is achievable with effective repair of welded joints. T-joints are often utilized in these structures to provide structural stability, keeping minimal body weight. Multi-pass friction stir welding (FSW) has proved to be useful for improving the quality of aluminium alloy welds employed in the aerospace sector. However, FSW of these alloys in T-configuration has not been sufficiently addressed yet. Even rarer is the discussion of efficacy of second FSW pass, with altered process parameters for improving the weld quality in T-joints. Hence, two commonly used aerospace grade aluminium alloys, namely, AA2024 and AA7075, were friction stir welded in T-configuration, varying three process parameters, i.e., tool rotational speed, welding speed and shoulder diameter. The effect of second FSW pass, performed at an optimum set of parameters, on kissing bond and tunnelling defect was studied in detail. A substantial reduction in the detrimental effect of these weld defects was discussed via tensile testing, micro-hardness and micro-structural observations.

Keywords: friction stir welding; T joints; second pass; defects; light alloys; AA2024; AA7075

1. Introduction

The safety and structural integrity of aircraft structures are largely dependent upon the skin-stringer joining [1–3]. T-joints in these structures enable a considerable increase in resistance against inertia and strength without substantial increase in weight, making them a vital component in the aerospace and transportation sectors [4]. The fabrication of skin-stringer welds using friction stir welding (FSW) not only eliminates the use of rivets [5], but also adds the benefits associated with this solid state joining technology, namely, zero porosity welds [6–8], low residual stresses [9], good dimensional stability [10], improved corrosion resistance [11], etc. Moreover, FSW has proved to be the most effective technology for joining aerospace grade aluminium alloys, mainly the 2xxx and 7xxx series in both similar and dissimilar arrangements [12–19]. Specifically, the joining of AA2024-T3 and AA7075-T6 alloys is commonly useful in the aerospace industry [20,21].

The main challenge faced during the T-section FSW is improper mixing between the skin and stringer metals. Previous studies have indicated that during the FSW of T-joints, mixing along the skin and stringer sections plays a key role in the determination of the weld quality [22–24]. Due to the same

reason, various defects like kissing bond, hooking and tunnels occur in the weld zone. A kissing bond is formed due to oxide layer retention at faying interface, which is caused primarily because of lack of sufficient heat and plastic deformation. Whereas, a tunnel is formed either due to (1) inadequate heating of the base metal leading to insufficient material flow, or (2) excessive softening and lack of consolidation of the metal in the solid phase joint. Zhao et al. [22] demonstrated the disparity in the effects of kissing bond and tunnelling defect in deterioration of the weld strength along the skin and stringer, respectively. It was established that an increase in the traverse speed results in larger voids and the kissing bond shifts towards the stir zone (SZ). However, if the kissing bond or oxide bands are located near the edges of the fillet zones, the weld strength decreases significantly [25]. Sato et al. [26] showed that no metallic bonding takes place on either side of the kissing bond line. Investigations with variation in shape (flat and curved) of the die corners (corners at both sides of the weld throat) and T-joint configuration, i.e., joint elements in two pieces and three pieces, have also been studied in detail.

In the past, research studies have resulted in an increase in weld properties, by employing multiple FSW passes at the same parameters [1,27–29]. Studies conducted by Sathari et al. [28] showed improved hardness, tensile strength and ductility for friction stir welds obtained via double pass, on comparison with the welds obtained through single pass. He et al. [1] concluded that the stability of the properties along the weld length improves after the double pass. A decrease in residual stress after multiple FSW passes has also been reported in the literature [27]. However, the potential for increase of friction stir weld properties by double pass has scarcely been utilized for dissimilar skin-stringer joining in general and 7xxx-2xxx combination in particular. Moreover, the effect of double pass in FSW, along with altered process parameters for the second pass has been accounted even more rarely. Further, most of the studies on FSW are focussed on welding in butt configuration. The nature of plasto-mechanics in the material required for successful FSW in T-configuration differs from that of butt configuration. Since a greater heat dissipation from the weld takes place due to clamping of the stringer, process parameters required to produce fine weldments are also different from those required in butt-welding [30,31]. Therefore, in the current study, two alloys vital for the aircraft industry, namely, AA2024-T3 and AA7075-T6, have been friction stir welded in T-joint configuration. The effect of second friction stir pass performed with changed process parameters upon the weld defects, micro-structural and mechanical properties has been addressed in detail.

2. Materials and Methods

FSW was performed in T-configuration, keeping AA2024-T3 alloy and AA7075-T6 alloy as skin and stringer materials, respectively. Since most applications of T-joints involve high strength material used as stringer [4], AA7075 alloy was kept as the stringer material. The dimensions of both the AA2024 and AA7075 alloy sheets were 200 mm × 50 mm × 2 mm. The chemical composition of these alloys is shown in Tables 1 and 2. Relevant mechanical and thermal properties are stated in Table 3. The incipient melting-liquidus temperature, thermal conductivity and specific heat capacity of the alloys has been obtained from the literature [32–36].

Table 1. Chemical composition of AA2024-T3 alloy (wt.%).

Element	Al	Cu	Mg	Si	Fe	Ni	Mn	Zn	Pb	Sn	Ti	Cr	V
Wt.%	Balance	4.62	1.10	0.062	0.133	0.014	0.438	0.03	0.004	0.012	0.027	<0.005	0.009

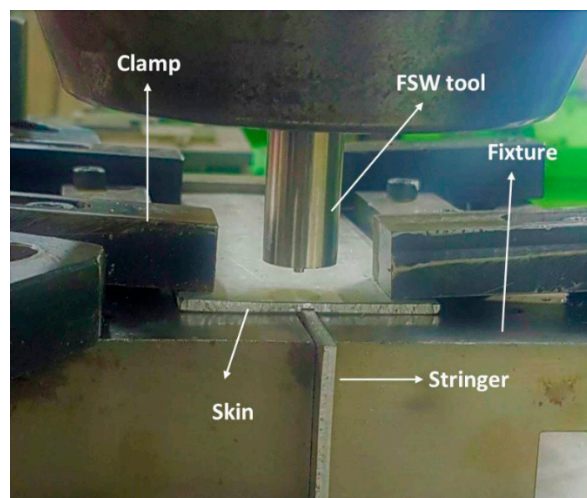
Table 2. Chemical composition of AA7075-T6 alloy (wt.%).

Element	Al	Cu	Mg	Si	Fe	Ni	Mn	Zn	Pb	Sn	Ti	Cr	V
Wt.%	Balance	1.6	2.74	0.051	0.127	<0.008	0.022	5.5	<0.001	0.005	0.024	0.218	0.008

Table 3. Thermal and Mechanical properties of AA2024-T3 and AA7075-T6 alloys.

Property	Aluminium Alloy	
	AA2024-T3	AA7075-T6
Ultimate Tensile Strength (MPa)	437	517
Vickers Hardness (HV)	168	225
Incipient melting-liquidus Temperature (°C)	502–638 °C	477–635 °C
Thermal Conductivity (W/(m·K))	121	130
Specific heat capacity (J/(g·°C))	0.875	0.96

A robust vertical milling machine with an indigenously developed fixture and tool adopter were utilized for carrying out FSW. An experimental setup, including the fixture used for clamping the skin and stringer plates, is shown in Figure 1.

**Figure 1.** Experimental setup for performing friction stir welding (FSW) in T-configuration.

A die corner radius of 2 mm was used to clamp the stringer. The fillet formed in the T-joint due to the die corners radius is necessary to avoid stress concentration at these sites [37]. High chromium high carbon steel was used for making the FSW tool. Tool pin failure due to process forces is another major challenge in the FSW of high strength aluminium alloys [38]. Continuous tapered pin profile with pin length 1.9 mm, a pin tip diameter 1.8 mm and pin root diameter 5.6 mm was selected after trial experimentation to induce effective material flow at the skin/stringer interface and prevent stress concentration at the root of the pin. The tool used for performing FSW and the transverse cross-section of weld geometry is schematically illustrated in Figure 2.

Three process parameters, namely, tool rotational speed, traverse speed and shoulder diameter, were varied across three levels. A Taguchi L9 orthogonal array was employed to design the experiments. Prior trial experimentation was also performed to identify the range of process parameters which yields sound welds.

Furthermore, to eliminate weld defects and enhance joint strength, second FSW pass was performed on welds obtained from Exp. Nos. 3 and 5. The type of defects found on advancing side (AS) and retreating side (RS) differ because of variation in material flow characteristics on the two sides. Similar flow kinematics during second pass can thus increase the size and detrimental effect of these defects. Therefore, the AS and RS were switched for the second FSW pass. These experiments have been termed as Exp. Nos. 3a and 5a, respectively. The parameters for double pass were kept same as those of Exp. No. 8. Peak tensile strength along stringer was selected as the criterion for selection of parameters for the second pass. The strategy behind this particular approach for second

pass has been addressed in detail in Section 3.1. Tool tilt angle was kept constant at 2°. Table 4 shows the experimental design for the current investigation.

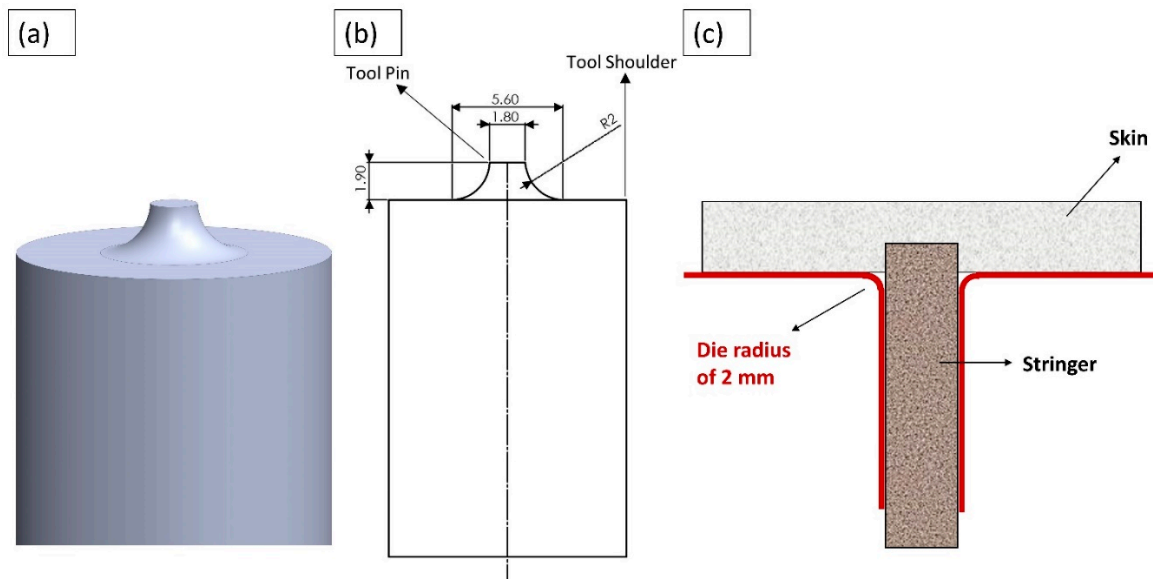


Figure 2. Schematic representation for (a) Tool 3D model (b) Tool Computer Aided Design (CAD) Drawing (c) Transverse weld cross-section (All dimensions are in mm).

Table 4. Experimental Design.

Experimental Design	Experiment Number	Process Parameter Level		
		Shoulder Diameter	Rotational Speed	Welding Speed
Taguchi L ₉	1	14	710	40
	2	16	710	50
	3	12	900	50
	4	12	560	40
	5	16	560	63
	6	14	900	63
	7	14	560	50
	8	12	710	63
	9	16	900	40
Second Pass	3a	12	710	63
	5a	12	710	63

A sample friction stir welded T-joint is shown in Figure 3.



Figure 3. A sample friction stir welded dissimilar T-joint.

The test specimens were cut using the CNC wire electric discharge machine (WEDM). The standard metallographic procedure was followed for micro-structural examination. The polished specimens were etched using 1.5 mL HNO_3 + 1 mL HF + 97.5 mL H_2O and observed under an optical microscope (OM). Vickers micro-hardness was measured on the transverse cross section, along the skin and stringer of the welded joint. Each indentation was made at a distance of 0.5 mm with axial load and dwell time of 100 gram and 15 s, respectively. Tensile strength of the T-joints was measured along the skin and stringer using a computer controlled Tensometer with 20 kN capacity. The parameter combination which yielded optimum tensile strength along the stringer was selected for the second pass. Tests were performed at room temperature and at a cross head speed of 2 mm/min. The fixtures used for tensile testing with the firmly fixed samples are shown in Figure 4.

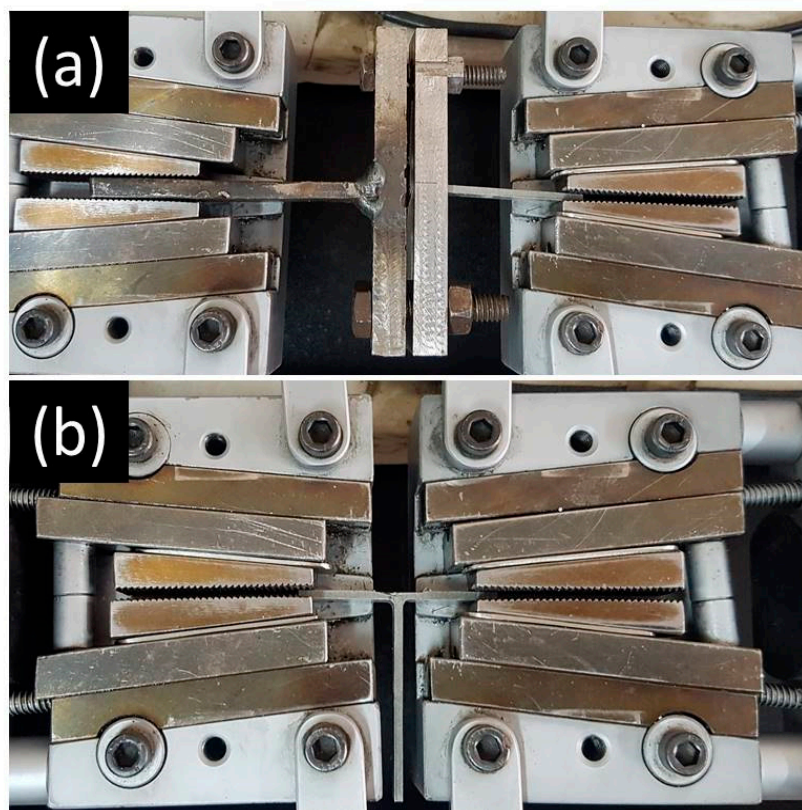


Figure 4. Fixtures used for tensile testing along (a) Stringer, (b) Skin.

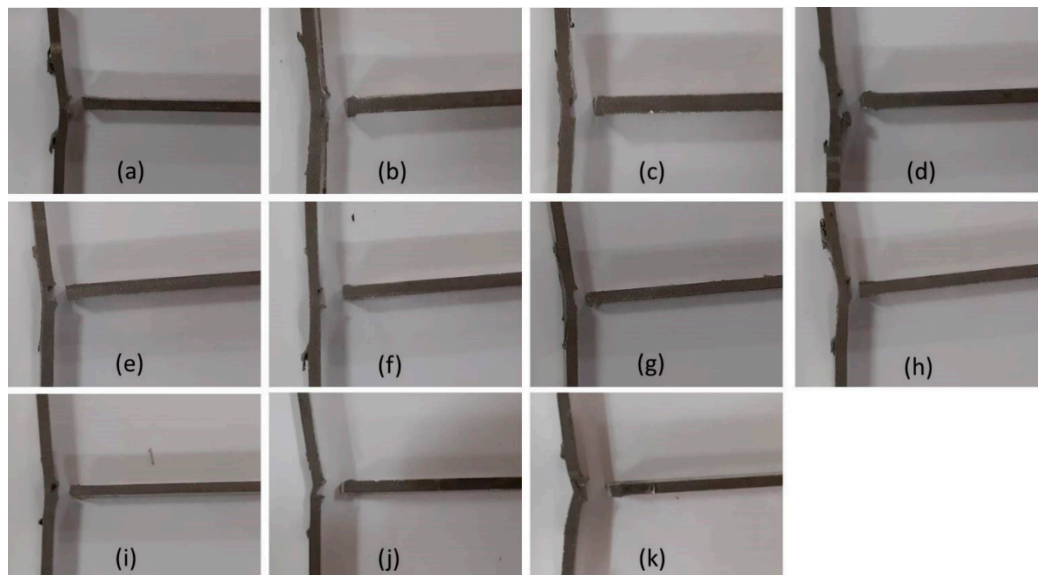
3. Results and Discussion

3.1. Tensile Strength

The tensile strength, percentage elongation and fracture location for all the welds along the skin and stringer have been shown in Table 5. The experiments have been classified according to their respective tool rotational speeds. The failed tensile specimen tested along the stringer and skin are shown in Figures 5 and 6, respectively. Apart from SZ, the specimen also failed from the thermo-mechanically affected zone (TMAZ), tunnel and the kissing bond (KB) defect. It can be clearly observed from Table 5 that a tool rotation speed of 710 rpm yields welds with relatively higher tensile strength and elongation along the skin and stringer. However, at a constant rotational speed, increase in tensile strength along the stringer is discernible with increasing welding speed, whereas no such pattern is visible for tensile strength along the skin. For single pass, a peak tensile strength (along skin) of 330 MPa was observed for Exp. No. 1 while maximum tensile strength along stringer (155 MPa) was observed for Exp. No. 8.

Table 5. Tensile Properties of welds tested along Skin and Stringer.

Exp. No.	Process Parameters			Tensile Properties along Skin			Tensile Properties along Stringer		
	N (rpm)	v (mm/min)	D (mm)	Tensile Strength (MPa)	Elongation (%)	Fracture Location	Tensile Strength (MPa)	Elongation (%)	Fracture Location
4	560	40	12	197	6.7	SZ	45	1.4	SZ
7	560	50	14	216	7.3	SZ	83	3.1	SZ
5	560	63	16	177	6.8	SZ	85	2.7	SZ
1	710	40	14	330	8.4	RS-TMAZ	71	2.8	SZ
2	710	50	16	303	10.9	SZ	108	3.2	SZ
8	710	63	12	258	10.2	RS-KB	155	4.3	SZ
9	900	40	16	209	6.9	SZ	42	1.8	SZ
3	900	50	12	150	6.2	Tunnel	53	2.2	SZ
6	900	63	14	265	7.0	AS-KB	63	2.3	SZ
3a	710	40	14	307	13.6	RS-KB	177	3.4	SZ
5a	710	40	14	273	7.7	RS-KB	165	5.6	SZ

**Figure 5.** Fractured tensile specimen tested along stringer for (a–i) Exp. Nos. 1–9 (j) Exp. No. 3a (k) Exp. No. 5a.

The second pass was strategically performed on the parameters which yielded optimum tensile strength along the stringer, i.e., Exp. No. 8. The effect of tool rotational speed on tensile strength was found to be dominant amongst the three parameters. Thus, to study the effect of second pass with altered process parameters from the scheme of first pass, one weld with lower and one weld with higher initial rotational speed than that of Exp. No. 8 were selected for second pass. At the rotational speeds of 560 rpm and 900 rpm, the welds with least tensile strength along the skin, i.e., Exp. Nos. 3 and 5, were chosen to achieve an overall improvement in the tensile properties of the welds. For the specimen incurring a tunnel defect, i.e., Exp. No. 3 (as shown in Section 3.2), an increase of more than 100% and 200% after the second pass was witnessed in the tensile strength along skin and stringer, respectively. Since Exp. No. 5 at the rotational speed of 560 rpm showed minimum strength along the skin, the second pass was performed on this weld. In this case, the tensile strength along skin improved from 177 MPa to 273 MPa, whereas along the stringer, the strength improved from 85 MPa to 165 MPa. The increase in tensile strength along the stringer for Exp. Nos. 3a and 5a demonstrates that the effect of kissing bond defect has decreased to a considerable degree after the second pass. A minimum rotational speed of 560 rpm does not generate sufficient heat to induce effective metallic bonding between the two base alloys. On the other hand, the highest rotational speed

of 900 rpm excessively softens the base alloy. As a result, the tool is not able to consolidate the material effectively, which ultimately lowers the tensile strength. Superimposing the optimum tool rotational speed of 710 rpm on these welds successfully eliminates these shortcomings, leading to the substantial enhancement of tensile properties.

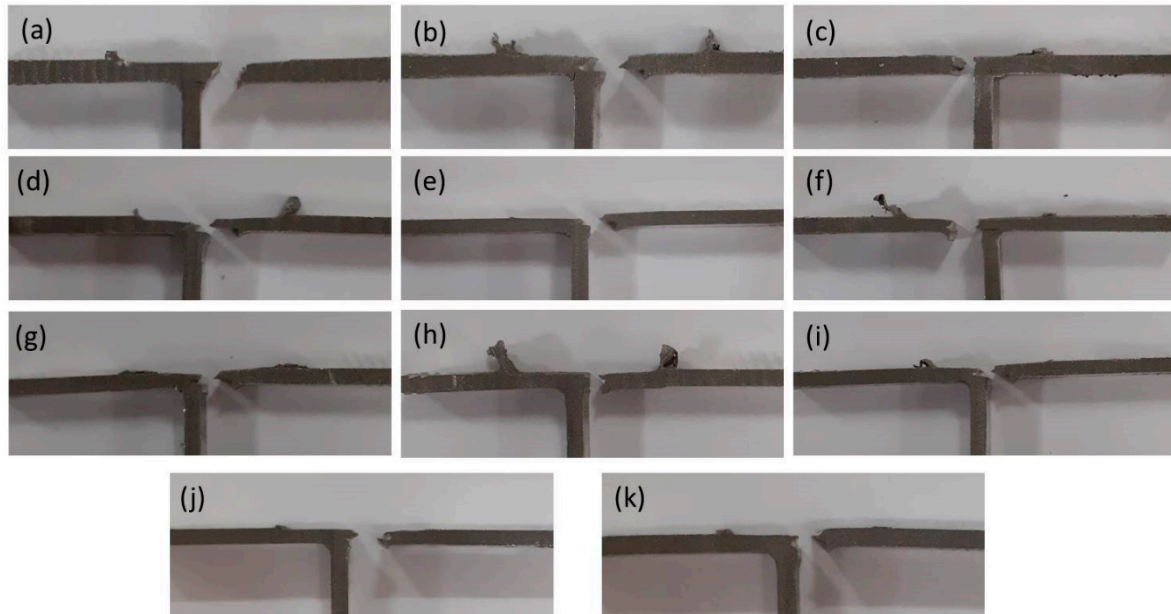


Figure 6. Fractured tensile specimen tested along skin for (a–i) Exp. Nos. 1–9 (j) Exp. No. 3a (k) Exp. No. 5a.

Along the stringer, all the welds failed from the interface of the two base alloys in SZ, as shown in Figure 5. Whereas, along the skin, 7 out of 9 welds from Taguchi L_9 experimental design failed from SZ, in such a manner that the stringer remained intact with the AS of skin section, as shown in Figure 6. This is principally due to better intermixing between the two alloys at the AS as compared to the RS. Furthermore, Exp. Nos. 3a and 5a can also be observed to adopt the failure location of Exp. No. 8, failing from the RS-KB. This is evident of the effective superimposition of material flow characteristics which improved the weld structure of Exp. Nos. 3 and 5, in coherence with the weld structure of Exp. No. 8.

3.2. Microstructure

The macrostructure of the weld obtained from Exp. No. 8 is shown in Figure 7. Figure 8 represents the corresponding micro-structures as observed under optical microscope. As it is well known for FSW, the weld structure consists of three different zones, namely, SZ, TMAZ and the heat affected zone (HAZ), which possess different mechanical properties and grain sizes. These zones can be distinctly demarcated in both the skin and stringer material of the welded joint, as shown in Figure 7. The interface of skin and stringer metals in the SZ can be observed in Figure 8a. The SZ experiences highest temperature and degree of plastic deformation, because of the stirring action of the tool, due to which the material undergoes dynamic recrystallization resulting in very fine, equi-axed grains. The TMAZ experiences comparatively smaller heat input and mainly undergoes induced plastic deformation. Since partial recrystallization occurs in the TMAZ, grains in this zone can be observed to be coarser than SZ. For both the materials, the HAZ consists of grains which are slightly larger than the base metal, because of the prevalent thermal cycle. It can be seen from Figure 7 that a broader SZ and thinner TMAZ exists for the stringer material as on the AS, in contrast to the steeper SZ and broader TMAZ in the RS. This elucidates the fact that a much higher degree of plastic deformation due to stirring occurs on the AS, in comparison with the RS.

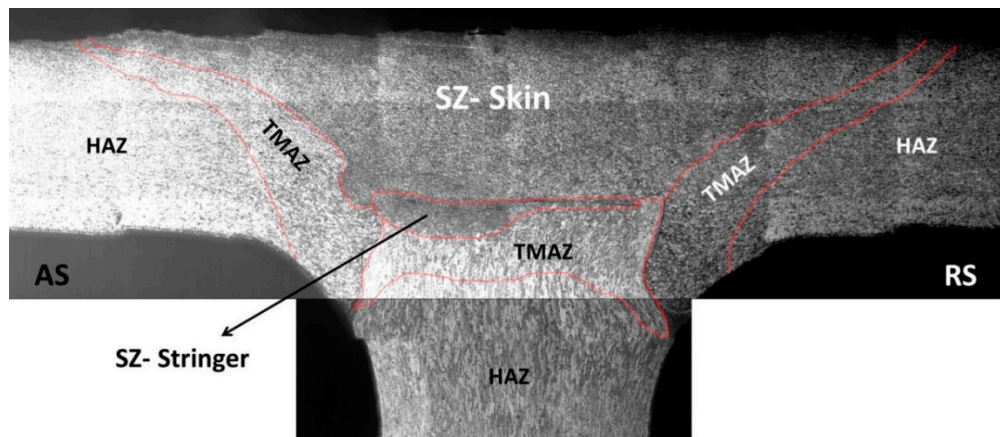


Figure 7. Macro-structure of weld obtained from Exp. No. 8.

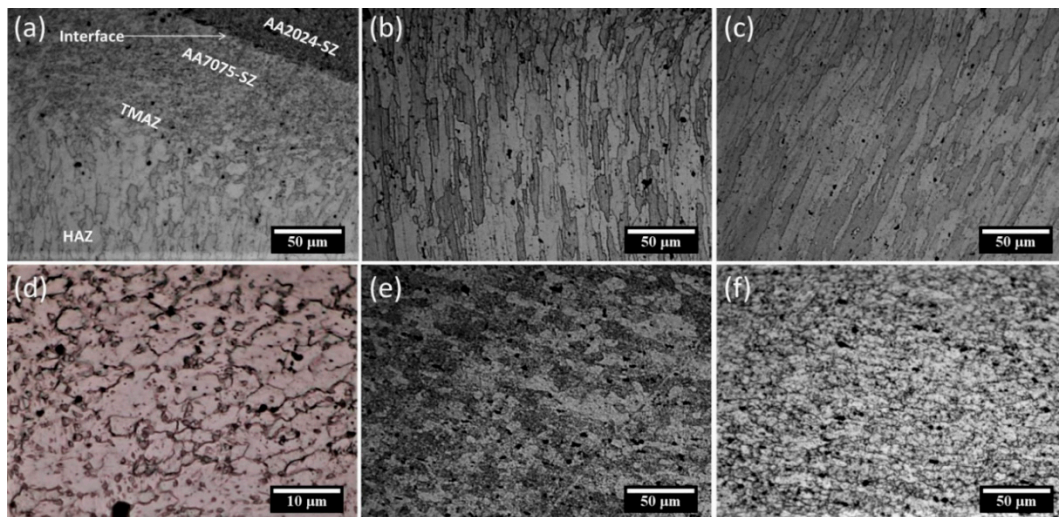


Figure 8. Micro-structure of weld zones obtained from Exp. No. 8 (a) Skin-stringer interface and various zones of stringer (b) HAZ-Stringer (c) Base alloy-Stringer (d) SZ-Skin (e) HAZ-Skin (f) Base alloy-Skin.

Figure 9 represents the presence of kissing bond (KB) defect on both AS and RS of the interface between the two alloys. A kissing bond can be seen where the base metals meet in the TMAZ regions. However, in the SZ, efficient intermixing in AS diminishes the kissing bond as explicit from Figure 9a. Whereas, the kissing bond remains obtrusive even in the SZ on the RS, due to a lower degree of plastic deformation.

Weld macro-structures for Exp. Nos. 3, 3a and 5, 5a are shown in Figures 10 and 11, respectively. A tunnel or void can be clearly seen on the AS of the skin/stringer interface in Figure 10a, which disappears after second pass. A very high heat input, due to the maximum rotational speed of 900 rpm in Exp. 3, plasticises a greater amount of material in the SZ. However, the smallest shoulder diameter of 12 mm appears unable to forge/consolidate this material effectively in the wake of the weld. As a result, the softened material would flow out of the weld in the form of flash, leading to metal deficiency and void in the SZ. Pishevar et al. [39] and Chen et al. [40] showed that the heat input during FSW is dominated by the rotational speed, in comparison with the other parameters, which also supports the above inference.

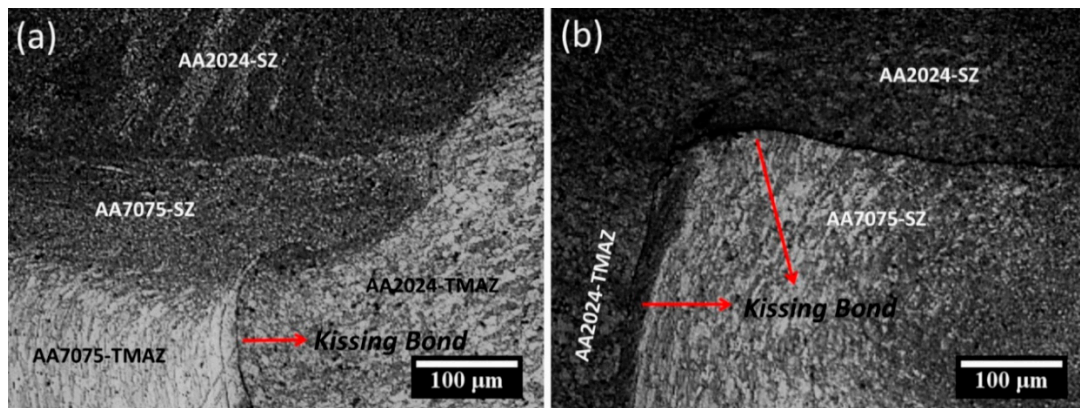


Figure 9. Kissing Bond defect at (a) AS and (b) RS at interface of skin and stringer.

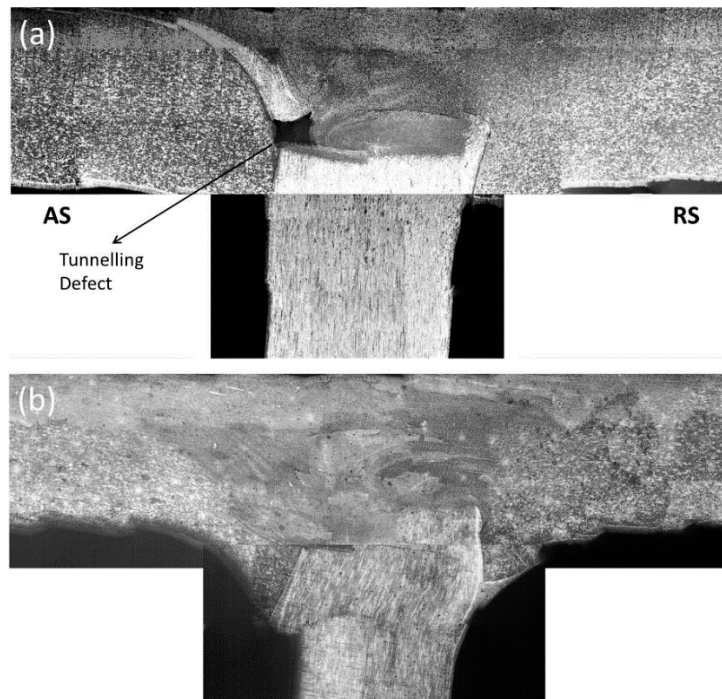


Figure 10. Macro-structure of weld obtained from (a) Exp. No. 3 (b) Exp. No. 3a.

Furthermore, a minimum rotational speed of 560 rpm was employed for Exp. No. 5, which results in lesser softening and the movement of material becomes difficult. As a result, higher flow stress prevails during welding. Notably and understandably, a tool tilt angle of 2° also influences the material flow dynamics in such a manner that upward extrusion and downward forging of base materials occurs on the AS and RS, respectively. Thus, the stringer material can be seen to be stretched upwards and skin material can be seen to be pulled downwards for Exp. No. 5 in Figure 11a. This also elucidates insufficient metallic bonding between the two materials, due to inadequate heat input. Importantly, an improvement in the homogenisation of AA2024-AA7075 intermixing is evident after the second pass for Exp. Nos. 3a and 5a. This homogenisation occurs due to the superimposition of more suitable material flow kinematics at optimum value of heat input. Since smaller values of flow stress exist for AA2024 as compared to AA7075 at identical temperatures, weld fillets have been formed by AA2024 in Exp. No. 8. However, due to the insufficient softening of AA2024, the AA7075 occupies the weld fillet in Exp. No. 5.

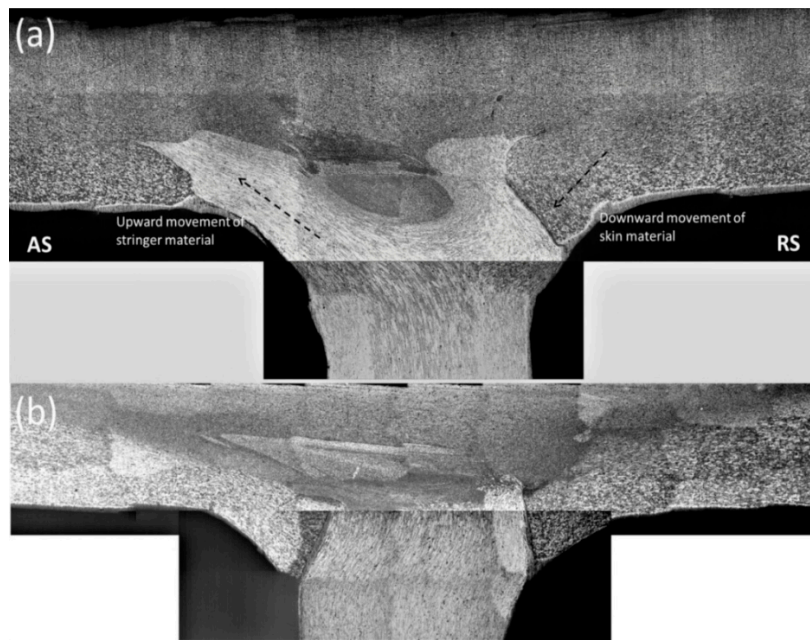


Figure 11. Macro-structure of weld obtained from (a) Exp. No. 5 (b) Exp. No. 5a.

3.3. Micro-Hardness

Micro-hardness distribution along the centre line of skin and stringer on the transverse cross-section for Exp. No. 8 is shown in Figures 12 and 13, respectively. Along the skin, the characteristic “W” plot for friction stir welded precipitate hardenable alloys can be clearly observed. As found out by various other researchers, the dissolution of strengthening precipitates causes reduction in hardness in the HAZ [41,42] and the grain refinement causes its relative increase in SZ [43]. It is worth noticing that the minimum micro-hardness of 103.4 HV exists at a distance of 8 mm from the weld centre on the AS, whereas in the stringer section, a minimum micro-hardness of 124.2 HV occurs at a distance of 9 mm from the weld centre. For AA2024, a maximum micro-hardness of 150.4 HV was observed in the SZ, which is comparable to that of the base alloy, i.e., 168 HV. However, the micro-hardness values in the welded AA7075 section range from 168.9 HV to 124.2 HV, which is considerably less than the base alloy micro-hardness of 225 HV. The above observation infers that amount of softening incurred by AA7075 alloy as stringer is much larger than AA2024 alloy as skin section.

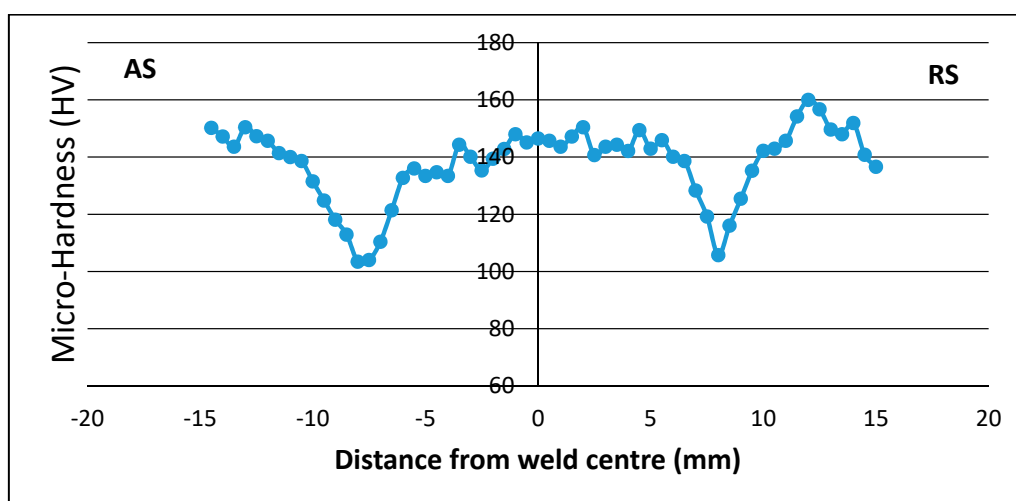


Figure 12. Micro-hardness distribution along skin for Exp. No. 8.

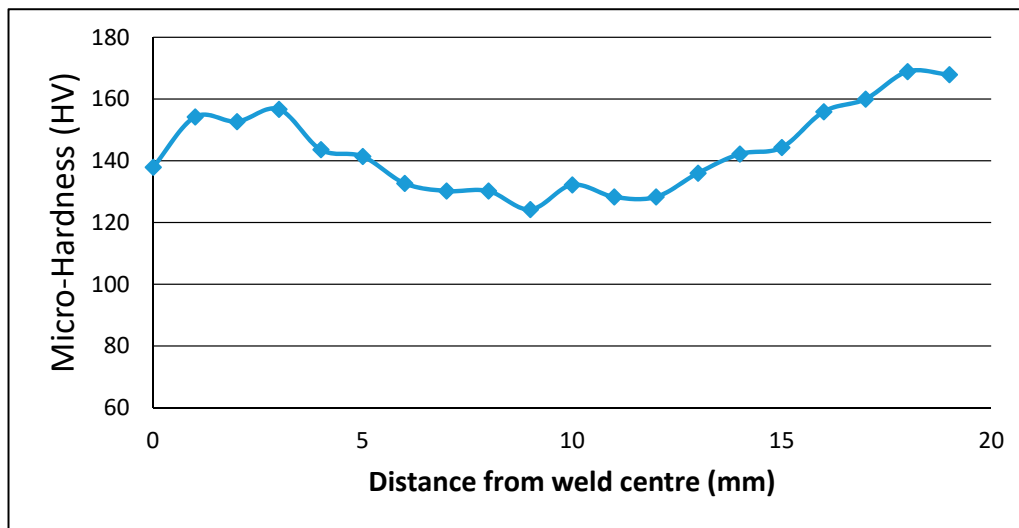


Figure 13. Micro-hardness distribution along stringer for Exp. No. 8.

Micro-hardness distribution along the skin section for Exp. Nos. 3 and 5, before and after the second pass is plotted in Figures 14 and 15, respectively. For Exp. No. 3, the hardness values in SZ after the second pass range from 117–126 HV, which is similar to the micro-hardness in SZ after the first pass. On the contrary, a significant decrease in micro-hardness values of SZ after the second pass for Exp. No. 5 is evident from Figure 15. This can be explained with reference to the rotational speed to which the welds were subjected in the first FSW pass. For Exp. No. 5, an increase in rotational speed occurs, from 560 rpm in the first pass to 710 rpm in the second pass. As discussed in Section 3.2, such a change in rotational speed leads to greater heat input in the second pass, which results in the better softening and higher degree of plastic deformation of SZ. However, this is not the case for Exp. Nos. 3 and 3a. Thus, such an observation has not been encountered for Exp. No. 3. The aberrant peaks in micro-hardness values in the SZ for Exp. No. 5a likely occur due to heterogeneous mixing with the harder stringer material, which can be observed in Figure 11. Notably, a considerable improvement in micro-hardness values occurs beyond the SZ after the second pass for both Exp. Nos. 3 and 5.

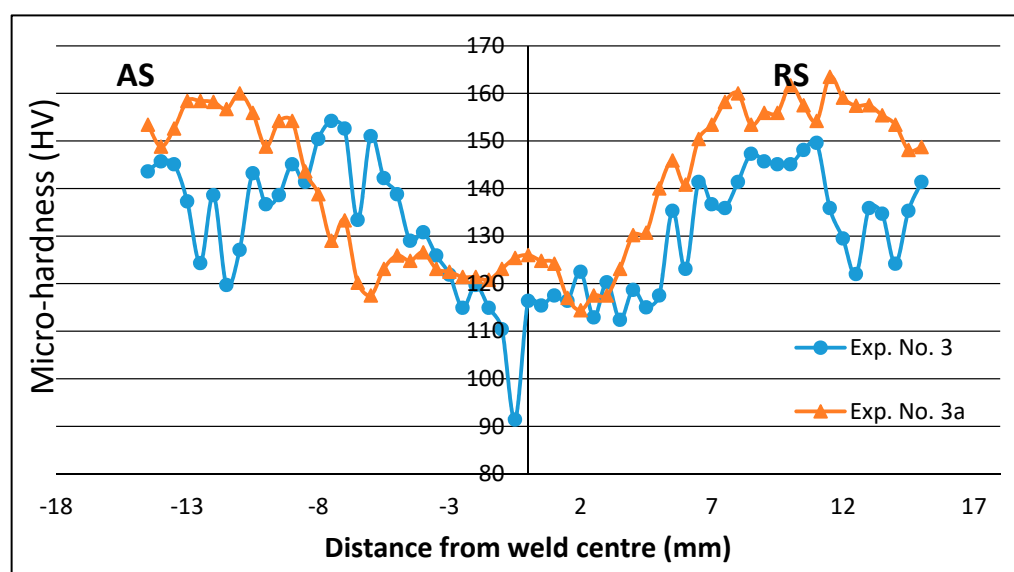


Figure 14. Micro-hardness distribution along skin for Exp. Nos. 3 and 3a.

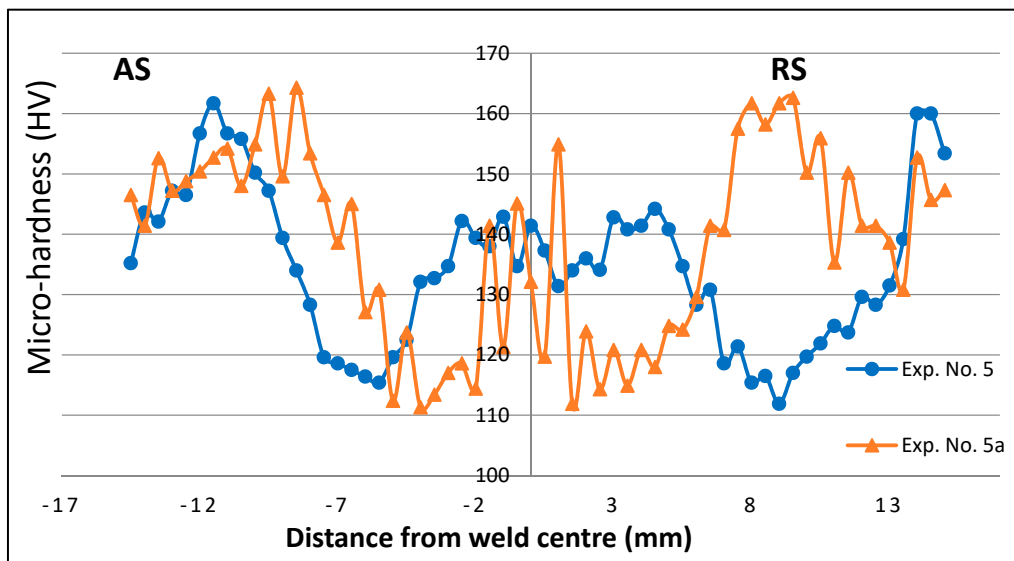


Figure 15. Micro-hardness distribution along skin for Exp. Nos. 5 and 5a.

The presence of a void in the SZ has also been reflected as a sudden fall of micro-hardness for Exp. No. 3.

4. Conclusions

In the present study, the effect of the second pass with altered process parameters on defects occurring in dissimilar T-friction stir welds was addressed, with reference to the mechanical and micro-structural features. The following conclusions can be drawn based upon the outcomes of this study:

(1) The tunnelling defect was eliminated and a significant decrement in the obtrusive effect of KB defect was achieved by applying second welding pass at optimum parameters which induced increased inter-mixing between the AA2024 and AA7075 alloys. A greater degree of plastic deformation at AS helps in overcoming KB defect at this side of the weld.

(2) A considerable decrease in micro-hardness of the SZ occurs when a higher tool rotational speed of 710 rpm was applied in the second pass. Whereas, when a lesser rotational speed than that of first pass is applied, a negligible change in the micro-hardness of SZ was encountered. The decrease in micro-hardness of the stringer alloy, i.e., AA7075 alloy, was much larger than the decrement in the hardness values of the AA2024 alloy. The appearance of aberrant peaks in micro-hardness distribution in SZ after the second pass indicate improved skin-stringer intermixing.

(3) For the weld exhibiting a void in the SZ in first pass, the ultimate tensile strength along skin increased from 150 MPa to 307 MPa after the second pass. Tensile strength along stringer also improved over 100% in comparison with the welds before the second pass. This positive restoration of weld structures occurs due to enhanced material flow dynamics at ideal heat input.

Author Contributions: Conceptualization, M.H.A., A.N.S., D.B. and M.A.; methodology, A.N.S., M.H.A., A.U.R.; formal analysis, D.B., N.A., H.I., S.A.; investigation, D.B., N.A., H.I., S.A.; resources, A.N.S., and M.H.A.; data curation, D.B., A.N.S., M.H.A.; writing—original draft preparation, A.N.S., D.B., M.A.; writing—review and editing, A.N.S., M.H.A., A.U.R.; supervision, A.N.S., M.A.; project administration, M.H.A., M.A., A.N.S.; funding acquisition, M.A., A.U.R. All authors have read and agreed to the published version of the manuscript.

Funding: This research was funded by Deanship of Scientific Research, King Saud University, through research group number RG-1439-027.

Acknowledgments: The authors extend their appreciation to the Deanship of Scientific Research at King Saud University for funding this work through research group number RG-1439-027.

Conflicts of Interest: The authors declare no conflict of interest.

References

1. He, D.; Yang, K.; Li, M.; Guo, H.; Li, N.; Lai, R.; Ye, S. Comparison of single and double pass friction stir welding of skin–stringer aviation aluminium alloy. *Sci. Technol. Weld. Join.* **2013**, *18*, 610–615. [[CrossRef](#)]
2. Teng, T.-L.; Fung, C.-P.; Chang, P.-H.; Yang, W.-C. Analysis of residual stresses and distortions in T-joint fillet welds. *Int. J. Press. Vessel. Pip.* **2001**, *78*, 523–538. [[CrossRef](#)]
3. Mashiri, F.R.; Zhao, X.-L.; Grundy, P. Stress concentration factors and fatigue behaviour of welded thin-walled CHS–SHS T-joints under in-plane bending. *Eng. Struct.* **2004**, *26*, 1861–1875. [[CrossRef](#)]
4. Tavares, S.M.O.; Castro, R.A.S.; Richter-Trummer, V.; Vilaça, P.; Moreira, P.M.G.P.; de Castro, P.M.S.T. Friction stir welding of T-joints with dissimilar aluminium alloys: Mechanical joint characterisation. *Sci. Technol. Weld. Join.* **2010**, *15*, 312–318. [[CrossRef](#)]
5. Mabuwa, S.; Msomi, V. Review on Friction Stir Processed TIG and Friction Stir Welded Dissimilar Alloy Joints. *Metals* **2020**, *10*, 142. [[CrossRef](#)]
6. Hannard, F.; Castin, S.; Maire, E.; Mokso, R.; Pardoën, T.; Simar, A. Ductilization of aluminium alloy 6056 by friction stir processing. *Acta Mater.* **2017**, *130*, 121–136. [[CrossRef](#)]
7. Ma, Z.Y.; Feng, A.H.; Chen, D.L.; Shen, J. Recent Advances in Friction Stir Welding/Processing of Aluminum Alloys: Microstructural Evolution and Mechanical Properties. *Crit. Rev. Solid State Mater. Sci.* **2018**, *43*, 269–333. [[CrossRef](#)]
8. Vilaça, P.; Santos, J.P.; Góis, A.; Quintino, L. Joining Aluminium Alloys Dissimilar in Thickness by Friction Stir Welding and Fusion Processes. *Weld. World* **2005**, *49*, 56–62. [[CrossRef](#)]
9. Prime, M.B.; Gnäupel-Herold, T.; Baumann, J.A.; Lederich, R.J.; Bowden, D.M.; Sebring, R.J. Residual stress measurements in a thick, dissimilar aluminum alloy friction stir weld. *Acta Mater.* **2006**, *54*, 4013–4021. [[CrossRef](#)]
10. Mishra, R.S.; Ma, Z.Y. Friction stir welding and processing. *Mater. Sci. Eng. R Rep.* **2005**, *50*, 1–78. [[CrossRef](#)]
11. Fahimpour, V.; Sadrnezhaad, S.K.; Karimzadeh, F. Corrosion behavior of aluminum 6061 alloy joined by friction stir welding and gas tungsten arc welding methods. *Mater. Des.* **2012**, *39*, 329–333. [[CrossRef](#)]
12. Kroninger, H.R.; Reynolds, A.P. R-curve behaviour of friction stir welds in aluminium-lithium alloy 2195. *Fatigue Fract. Eng. Mater. Struct.* **2002**, *25*, 283–290. [[CrossRef](#)]
13. Shercliff, H.R.; Russell, M.J.; Taylor, A.; Dickerson, T.L. Microstructural modelling in friction stir welding of 2000 series aluminium alloys. *Mech. Ind.* **2005**, *6*, 25–35. [[CrossRef](#)]
14. Gupta, R.K.; Das, H.; Pal, T.K. Influence of Processing Parameters on Induced Energy, Mechanical and Corrosion Properties of FSW Butt Joint of 7475 AA. *J. Mater. Eng. Perform.* **2012**, *21*, 1645–1654. [[CrossRef](#)]
15. Kadlec, M.; Růžek, R.; Nováková, L. Mechanical behaviour of AA 7475 friction stir welds with the kissing bond defect. *Int. J. Fatigue* **2015**, *74*, 7–19. [[CrossRef](#)]
16. Arora, K.S.; Pandey, S.; Schaper, M.; Kumar, R. Effect of process parameters on friction stir welding of aluminum alloy 2219-T87. *Int. J. Adv. Manuf. Technol.* **2010**, *50*, 941–952. [[CrossRef](#)]
17. Sheng, X.; Li, K.; Wu, W.; Yang, Y.; Liu, Y.; Zhao, Y.; He, G. Microstructure and Mechanical Properties of Friction Stir Welded Joint of an Aluminum Alloy Sheet 6005A-T4. *Metals* **2019**, *9*, 1152. [[CrossRef](#)]
18. Vidal, C.; Infante, V. Fatigue behavior of friction stir-welded joints repaired by grinding. *J. Mater. Eng. Perform.* **2004**, *23*, 1340–1349. [[CrossRef](#)]
19. Cabibbo, M.; Forcelllese, A.; Santecchia, E.; Paoletti, C.; Spigarelli, S.; Simoncini, M. New Approaches to Friction Stir Welding of Aluminum Light-Alloys. *Metals* **2020**, *10*, 233. [[CrossRef](#)]
20. Cederqvist, L.; Reynolds, A. Factors affecting the properties of friction stir welded aluminum lap joints. *Weld. J.* **2001**, *80*, 281-s.
21. Cavaliere, P.; Nobile, R.; Panella, F.W.; Squillace, A. Mechanical and microstructural behaviour of 2024–7075 aluminium alloy sheets joined by friction stir welding. *Int. J. Mach. Tools Manuf.* **2006**, *46*, 588–594. [[CrossRef](#)]
22. Zhao, Y.; Zhou, L.; Wang, Q.; Yan, K.; Zou, J. Defects and tensile properties of 6013 aluminum alloy T-joints by friction stir welding. *Mater. Des.* **2014**, *57*, 146–155. [[CrossRef](#)]
23. Boz, M.; Kurt, A. The influence of stirrer geometry on bonding and mechanical properties in friction stir welding process. *Mater. Des.* **2004**, *25*, 343–347. [[CrossRef](#)]
24. Fratini, L.; Micari, F.; Squillace, A.; Giorleo, G. Experimental Characterization of FSW T-Joints of Light Alloys. *Key Eng. Mater.* **2007**, *344*, 751–758. [[CrossRef](#)]

25. Krasnowski, K. Experimental Study of FSW T-joints of EN-AW 6082-T6 and Their Behaviour Under Static Loads. *Arab. J. Sci. Eng.* **2014**, *39*, 9083–9092. [[CrossRef](#)]
26. Sato, Y.S.; Takauchi, H.; Park, S.H.C.; Kokawa, H. Characteristics of the kissing-bond in friction stir welded Al alloy 1050. *Mater. Sci. Eng. A* **2005**, *405*, 333–338. [[CrossRef](#)]
27. Brown, R.; Tang, W.; Reynolds, A.P. Multi-pass friction stir welding in alloy 7050-T7451: Effects on weld response variables and on weld properties. *Mater. Sci. Eng. A* **2009**, *513–514*, 115–121. [[CrossRef](#)]
28. Sathari, N.A.; Shah, L.H.; Razali, A.R. Investigation of single-pass/double-pass techniques on friction stir welding of aluminium. *J. Mech. Eng. Sci.* **2014**, *7*, 1053–1061. [[CrossRef](#)]
29. Osman, N.; Sajuri, Z.; Baghdadi, A.H.; Omar, M.Z. Effect of Process Parameters on Interfacial Bonding Properties of Aluminium–Copper Clad Sheet Processed by Multi-Pass Friction Stir-Welding Technique. *Metals* **2019**, *9*, 1159. [[CrossRef](#)]
30. Erbslöh, K.; Dalle Donne, C.; Lohwasser, D. Friction Stir Welding of T-Joints. *Mater. Sci. Forum* **2003**, *426–432*, 2965–2970. [[CrossRef](#)]
31. Chen, Y.; Li, H.; Wang, X.; Ding, H.; Zhang, F. A Comparative Investigation on Conventional and Stationary Shoulder Friction Stir Welding of Al-7075 Butt-Lap Structure. *Metals* **2019**, *9*, 1264. [[CrossRef](#)]
32. Information Provided by The Aluminum Association, Inc. from Aluminum Standards and Data 2000 and/or International Alloy Designations and Chemical Composition Limits for Wrought Aluminum and Wrought Aluminum Alloys (Revised 2001). Available online: <http://asm.matweb.com/search/SpecificMaterial.asp?bassnum=MA2024T3> (accessed on 17 April 2020).
33. Baucio, M. (Ed.) *ASM Metals Reference Book*, 3rd ed.; ASM International: Materials Park, OH, USA, 1993.
34. *Metals Handbook*, 10th ed.; Vol.2—Properties and Selection: Nonferrous Alloys and Special-Purpose Materials; ASM International: Materials Park, OH, USA, 1990.
35. Howard, E.B.; Timothy, L.G. (Eds.) *Metals Handbook*; American Society for Metals: Materials Park, OH, USA, 1985.
36. John, M.T.H.; HO, C.Y. (Eds.) *Structural Alloys Handbook*, 1996th ed.; CINDAS/Purdue University: West Lafayette, IN, USA, 1996.
37. Fratini, L.; Buffa, G.; Shivpuri, R. Influence of material characteristics on plastomechanics of the FSW process for T-joints. *Mater. Des.* **2009**, *30*, 2435–2445. [[CrossRef](#)]
38. Arora, A.; Mehta, M.; De, A.; DebRoy, T. Load bearing capacity of tool pin during friction stir welding. *The Int. J. Adv. Manuf. Technol.* **2012**, *61*, 911–920. [[CrossRef](#)]
39. Pishevar, M.R.; Mohandesi, J.A.; Omidvar, H.; Safarkhanian, M.A. Influences of Friction Stir Welding Parameters on Microstructural and Mechanical Properties of AA5456 (AlMg5) at Different Lap Joint Thicknesses. *J. Mater. Eng. Perform.* **2015**, *24*, 3835–3844. [[CrossRef](#)]
40. Chen, Y.; Ding, H.; Li, J.-Z.; Zhao, J.-W.; Fu, M.-J.; Li, X.-H. Effect of welding heat input and post-welded heat treatment on hardness of stir zone for friction stir-welded 2024-T3 aluminum alloy. *Trans. Nonferrous Met. Soc. China* **2015**, *25*, 2524–2532. [[CrossRef](#)]
41. Leitao, C.; Leal, R.M.; Rodrigues, D.M.; Loureiro, A.; Vilaça, P. Mechanical behaviour of similar and dissimilar AA5182-H111 and AA6016-T4 thin friction stir welds. *Mater. Des.* **2009**, *30*, 101–108. [[CrossRef](#)]
42. Khodir, S.A.; Shibayanagi, T. Friction stir welding of dissimilar AA2024 and AA7075 aluminum alloys. *Mater. Sci. Eng. B* **2008**, *148*, 82–87. [[CrossRef](#)]
43. Yan, Z.; Liu, X.; Fang, H. Effect of Sheet Configuration on Microstructure and Mechanical Behaviors of Dissimilar Al–Mg–Si/Al–Zn–Mg Aluminum Alloys Friction Stir Welding Joints. *J. Mater. Sci. Technol.* **2016**, *32*, 1378–1385. [[CrossRef](#)]

